Carbon storage in the mid-depth Atlantic during millennial-scale climate events

Matthew Lacerra[1], David Lund[1*], Jimin Yu[2], and Andreas Schmittner[3]

[1] Dept. of Marine Sciences, University of Connecticut, 1080 Shennecossett Rd., Groton, CT, 06340 USA
[2] Research School of Earth Sciences, Australian National University, Acton ACT 2601, Australia
[3] College of Earth, Ocean, and Atmospheric Sciences, Oregon State University, 104 CEOAS Admin. Bldg., Corvallis, OR 97331 USA

[*] Corresponding author (david.lund@uconn.edu, 860-405-9331)

Abstract

Carbon isotope minima were a ubiquitous feature of the mid-depth Atlantic during Heinrich Stadial 1 (HS1, 14.5-17.5 kyr BP) and the Younger Dryas (YD, 11.5-12.9 kyr BP) yet their cause remains unclear. Recent evidence indicates that North Atlantic processes triggered the $\delta^{13}C$ anomalies, with weakening of the Atlantic Meridional Overturning Circulation (AMOC) being the most likely driver. Model simulations suggest slowing of the AMOC increases the residence time of mid-depth waters in the Atlantic, resulting in the accumulation of respired carbon. Here we assess ΣCO_2 storage in the South Atlantic using benthic foraminiferal B/Ca, a proxy for $[CO_3^{2-}]$. Using replicated high resolution B/Ca records from ~ 2 km water depth on the Brazil Margin, we show that $[CO_3^{2-}]$ decreased during HS1 and the YD, synchronous with apparent weakening of the AMOC. The $[CO_3^{2-}]$ response is smaller than in the tropical North Atlantic during HS1, indicating there was a north-south gradient in the $[CO_3^{2-}]$ signal similar to that for $\delta^{13}C$. The implied variability in ΣCO_2 is consistent with model results, suggesting that carbon is temporarily sequestered in the mid-depth Atlantic during millennial-scale stadial events. Using a carbon isotope mass balance, we estimate that approximately 75% of the HS1 $\delta^{13}C$ signal at the Brazil Margin was driven by accumulation of remineralized carbon, highlighting the non-conservative behavior of $\delta^{13}C$ during the last deglaciation.

1. Introduction

The last deglaciation (10-18 kyr BP) was characterized by major changes in the Earth's climate system, including a 120 m rise in global sea level (Clark et al., 2009), a ~ 4°C increase in average temperature (Shakun et al, 2012; Annan and Hargreaves, 2013), and an 80 ppmv increase in atmospheric CO_2 (Marcott et al., 2014). Given that global temperature tracked CO_2 levels (Shakun et al., 2012) and that greenhouse gases are necessary to simulate the full deglacial temperature rise (Weaver et al., 1998; Schneider et al., 2010), isolating the mechanisms that regulate atmospheric CO_2 is essential to understanding Earth's transition from a glacial to interglacial state.

The initial changes in deglacial climate occurred during Heinrich Stadial 1 (HS1, 14.5-17.5 kyr BP), including a 30 ppmv rise in pCO_2 and a decrease in the $\delta^{13}C$ of CO_2 of 0.3-0.4‰ (Lourantou et al., 2010; Schmitt et al., 2012; Bauska et al., 2016). Foraminiferal records also show that decreases in $\delta^{13}C$ were widespread in the surface and mid-depth (1.5-2.5 km) Atlantic Ocean (Curry et al., 1988; Schneider et al., 1992; Oppo et al., 2015). The largest anomalies occurred in the subpolar North Atlantic (McManus et al., 1999; Rickaby and Elderfield, 2005; Praetorius et al., 2008), with progressively smaller $\delta^{13}C$ excursions in the tropical (Zahn and Stuber, 2002; Oppo and Fairbanks, 1987) and South Atlantic (Tessin and Lund, 2013; Lund et al., 2015). The timing of the mid-depth $\delta^{13}C$ signals is similar to the atmospheric $\delta^{13}C$ anomaly, suggesting that circulation changes in the Atlantic played a key role in spurring the initial rise of atmospheric CO_2 during the last deglaciation (Oppo et al., 2015; Schmittner and Lund, 2015).

Several mechanisms have been proposed to explain HS1 $\delta^{13}C$ anomalies in the Atlantic, including regional brine formation (Dokken and Jansen, 1999; Thornalley et al., 2010; Waelbroeck et al., 2011), greater incursion of Antarctic Intermediate Water (AAIW) (Rickaby & Elderfield, 2005), and weakening of the AMOC (Zahn et al., 1997). Although the abyssal South Atlantic was depleted in ^{13}C during the LGM (Duplessy et al., 1988; Curry and Oppo, 2005; Hoffman & Lund, 2012), it is an unlikely source of mid-depth anomalies because the $\delta^{13}C$ signal in the abyssal and mid-depth records is offset by several thousand years (Lund et al., 2015). Moreover, the idea that greater incursion of AAIW caused the HS1 minima is now considered unlikely, as new records suggest a reduced presence of AAIW in the North Atlantic during this time (Xie et al., 2012; Huang et al., 2014). Greater incursion of AAIW should also lead to lower $\delta^{13}C$ at intermediate depths, which is opposite the pattern observed at multiple sites in the southern hemisphere, including the Brazil margin (Hertzberg et al., 2016). Instead, the mid-depth anomalies are most likely due to a change in the isotopic composition of northern component water (NCW) (Oppo et al., 2015). The end-member $\delta^{18}O$ and $\delta^{13}C$ values for NCW exhibited a significant change during the LGM-HS1 transition (-1.2 ‰ and -1.0 ‰, respectively), while end-member values for deep southern sourced water remained relatively stable (Lund et al., 2015). Cross plots of benthic $\delta^{13}C$ vs. $\delta^{18}O$ suggest that mid-depth Brazil Margin sites fall on a mixing line between NCW and deep (2500-3000 m) southern component water during HS1, implying that variable NCW composition caused the mid-depth anomalies (Lund et al., 2015). Similarly, a compilation of Atlantic LGM $\delta^{13}C$ vs. LGM-HS1 $\delta^{13}C$ indicates that NCW was the primary driver of the HS1 signal (see Figure 5 in Oppo et al., 2015).

73 Model simulations suggest the shift in NCW during HS1 was due to a severe reduction in
74 the AMOC. Shutdown of the AMOC by freshwater forcing in the North Atlantic yields negative
75 $\delta^{13}C$ anomalies at mid-depth, with the largest signal occurring in the high latitude North Atlantic
76 and progressively smaller anomalies in the tropical and South Atlantic, similar to the observed
77 spatial trend during HS1 (Schmittner & Lund 2015). The $\delta^{13}C$ response is due to reduced sinking
78 of high $\delta^{13}C$ surface water in the North Atlantic and increased residence time of deep water,
79 which allows for the accumulation of isotopically light respired carbon. Under modern
80 conditions, the North Atlantic has high $\delta^{13}C$ values due to sinking of ^{13}C-enriched surface waters
81 and rapid transport of deep water by the AMOC, while the South Atlantic has lower $\delta^{13}C$ due to
82 mixing with ^{13}C-depleted Upper Circumpolar Deep Water and Antarctic Bottom Water
83 (Kroopnick, 1985; Schmittner et al., 2013). The simulated shutdown of the AMOC nearly
84 eliminates this gradient, making the Atlantic $\delta^{13}C$ tracer field similar to the modern deep Pacific
85 where remineralization is the primary driver of $\delta^{13}C$ variability (Schmittner and Lund, 2015).
86
87 Although the modeled Atlantic response generally agrees with the observed spatial
88 pattern in $\delta^{13}C$ anomalies, the simulated signal in the North Atlantic is approximately 50% larger
89 than in the benthic $\delta^{13}C$ records. Bioturbation may mute the reconstructed signal in low
90 sedimentation rate locations, but both high and low resolution records yield smaller than
91 predicted anomalies in the North Atlantic (Schmittner and Lund, 2015). The discrepancy may
92 instead be related to the initial conditions used in the AMOC simulations, which were based on a
93 pre-industrial rather than LGM climate state. Another possibility is that the Atlantic overturning
94 did not fully collapse during HS1. While initial $^{231}Pa/^{230}Th$ records from the North Atlantic
95 pointed towards a complete AMOC shutdown (McManus et al., 2004), newer results are

consistent with the continued export of ^{231}Pa out of the North Atlantic (Gherardi et al., 2009). Furthermore, the Pa/Th proxy is influenced by spatially variable particle scavenging, indicating it may not be a direct quantitative indicator of AMOC flux (Hayes et al., 2015).

A key unknown is whether the mid-depth carbon isotope anomalies were driven by changes in preformed or remineralized carbon. If temperature dependent air-sea equilibration (e.g. Lynch-Steiglitz, 1995) was the primary driver of the $\delta^{13}C$ signal, we would expect little change in ΣCO_2 at mid-depths. On the other hand, a substantial increase in ΣCO_2 would point to either: 1) accumulation of respired carbon, due to weakening of the AMOC, or 2) higher preformed DIC, due to rising atmospheric CO_2. If it was the former, we would expect higher ΣCO_2 during HS1 and lower ΣCO_2 during the Bølling-Allerød (B-A, 12.9-14.5 kyr BP), whereas the latter should yield a monotonic increase in ΣCO_2 during the deglaciation. One existing record from the tropical North Atlantic (~12°N; 1800 m) shows that $[CO_3^{2-}]$ decreased by ~30 μmol/kg during the LGM-HS1 transition and remained low into the Holocene (Yu et al., 2010). Assuming alkalinity (ALK) remained constant and $[CO_3^{2-}] \approx 0.6*(ALK - \Sigma CO_2)$ (Yu et al., 2016), these results suggest ΣCO_2 increased by ~50 μmol/kg, which is inconsistent with temperature-dependent fractionation causing the mid-depth $\delta^{13}C$ anomalies. However, it leaves open the possibility that the $[CO_3^{2-}]$ signal was driven by preformed DIC. One of the goals of this work is to verify the North Atlantic results using new records from locations influenced by the AMOC that are capable of resolving millennial-scale $[CO_3^{2-}]$ variability during the deglaciation.

Here, we reconstruct [CO_3^{2-}] in the Southwest Atlantic using B/Ca analyses of benthic foraminifera from two mid-depth cores on the Brazil Margin (at 1.8 km and 2.1 km water depth) (Figure 1). During the LGM, water at these depths was approximately 70% NCW and 30% Antarctic Bottom Water (Tessin and Lund, 2013; Curry and Oppo; 2005), while during the Holocene the primary endmember influences were NADW and UCDW (Hoffman and Lund, 2012). The cores have accumulation rates of ~30 cm/kyr which allows for high-resolution (200-300 year) reconstruction of [CO_3^{2-}], which we use to infer changes in ΣCO_2. We use [CO_3^{2-}] estimates and $\delta^{13}C$ records from the same cores to infer the preformed and remineralized components of the HS1 $\delta^{13}C$ anomalies. We also evaluate the Brazil Margin records in the context of [CO_3^{2-}] and circulation proxies from the North Atlantic to assess the relative timing of events and whether variable AMOC strength drove changes in carbon storage at mid-depths. Finally, we discuss the implications of our findings as they relate to the HS1 carbon isotope minima and centennial to millennial-scale changes in atmospheric CO_2. It has been hypothesized that release of stored carbon due to reinvigoration of the AMOC may explain the abrupt 10-15 ppm increases in atmospheric CO_2 at the end of HS1 and the YD (Chen et al., 2015). One objective of this study is to assess whether carbon was temporarily sequestered at mid-depths using the Brazil Margin records.

2. Methods

2.1. Core Sampling

Sediment samples were taken from two cores on the Brazil Margin, KNR159-5-78GGC (1820 m; 27.5°S, 46.3°W) and KNR159-5-33GGC (2082 m; 27.6°S, 46.2°W). In core 78GGC,

141 samples were collected at 2 cm intervals from the core top to 61 cm, and then 4 cm intervals
142 from 61 cm to 201 cm (for a total of 68 samples). Note that two of the samples (at 73 cm and 77
143 cm) were collected within the bioturbated interval from 70-80 cm (Tessin and Lund, 2013). We
144 collected a total of 42 samples from 33GGC, ranging from 2 cm intervals from the core top to 59
145 cm and then 4 cm intervals from 59 cm to 199 cm, with the exception of 118 cm to 143 cm,
146 where the average sampling interval was 12 cm. The varied sample spacing in each core was
147 necessary to compensate for generally lower sedimentation rates in the Holocene and late
148 deglacial sections of each core. According the age models published in Tessin and Lund (2013),
149 the upper 50 cm of 78GGC has sedimentation rates of 3 cm/kyr, while below 50 cm the rate is
150 approximately 35 cm/kyr. Similarly, sedimentation rates in the upper 75 cm of core 33GGC are
151 2 cm/kyr, while deeper in the core the rate is ~27 cm/kyr. In total, we collected 86 samples from
152 78GGC and 51 samples from core 33GGC for B/Ca analyses. Samples were freeze-dried,
153 washed through a 150 μm sieve and dried at 40ºC overnight.
154
155 **2.2. B/Ca**
156 B/Ca analyses were performed on the benthic foraminifera *Cibicidoides wuellerstorfi* in
157 the laboratory of Dr. Jimin Yu at Australian National University. *C. wuellerstorfi* were taken
158 from the >250 μm size fraction with 5–8 tests used for each B/Ca analysis. Samples were
159 crushed using glass microscope slides with just enough force to rupture individual chambers. A
160 compound light microscope was used to facilitate the crushing procedure and the removal of
161 exceptionally dirty chambers. Crushed samples were rinsed into sample vials using Milli-Q
162 water and ultra-sonicated for 30 seconds to bring any clay material into suspension. The mixture
163 was then stirred by squirting Milli-Q into each vial. After test fragments had resettled the

overlying fluid was pipetted out. This procedure was repeated with Milli-Q and then methanol rinses until sonication yielded a clear, particle free supernatant. Using a high powered reflected-light microscope, we used a single haired picking brush to remove pyrite and other foreign materials from test fragments that remained after the rinsing procedure. The samples then underwent oxidative cleaning to remove organic matter using a buffered H_2O_2 solution (100µL 30%v/v H_2O_2 + 10mL 0.1M NaOH). The final step of the cleaning protocol involved leaching using a weak acid solution (0.001M HNO_3). Cleaned samples were analyzed for B/Ca using a Varian ICP 820MS. The analytical precision for the 150 µmol/mol B/Ca consistency standard analyzed with the unknowns was 1.6% (n=16). Full details of the analytical procedure can be found in Yu et al. (2005).

2.3. $[CO_3^{2-}]$ and ΣCO_2

Modern carbonate ion concentrations for the Brazil Margin were estimated using the local and regional hydrographic parameters listed in Table 1. Potential temperature and salinity values were taken directly from cruise KNR159-5 CTD data. PO_4^{3-} and SiO_3^{2-} values were estimated using WOCE Atlas Volume 3, Section A10, which intersects the Brazil Margin at 28°S (http://whpatlas.ucsd.edu/whp_atlas/atlantic/a10/sections/sct_menu.htm). ALK and ΣCO_2 values were estimated using WOCE data from stations 13003 (43.58°W, 28.83°S) and 13627 (46.48°W, 27.95°S), located approximately 300 km and 60 km from the core sites, respectively (http://www.ewoce.org/data/index.html#WHP_Bottle_Data). Given sloping isopycnals between the WOCE stations and the core locations, ALK and ΣCO_2 values were estimated using station data within ±0.05 kg/m^3 of the potential density at each core site. Using the data in Table 1, we then estimated $[CO_3^{2-}]$ using CO2SYS_v1.1 (Lewis & Wallace, 2014). Carbonate ion saturation

187 values were determined using the equation $[CO_3^{2-}]_{sat} = [CO_3^{2-}] / \Omega_{calcite}$, where $\Omega_{calcite}$ is the
188 saturation state for calcite at the depth of each core.
189
190 Down core estimates of $[CO_3^{2-}]$ were determined using a B/Ca to $\Delta[CO_3^{2-}]$ conversion of
191 1.14 (μmol/mol) B/Ca per (μmol/kg) $\Delta[CO_3^{2-}]$ (Yu and Elderfield, 2007). This relationship is
192 based on a global core-top calibration for *C. wuellerstorfi*. We then estimated $[CO_3^{2-}]$ using the
193 relationship $[CO_3^{2-}] = \Delta[CO_3^{2-}] + [CO_3^{2-}]_{sat}$, where $[CO_3^{2-}]_{sat}$ is based on modern hydrographic
194 conditions and water depths (Table 1). Our estimates of ΣCO_2 are based on the carbonate
195 alkalinity relationship $\Sigma CO_2 \approx ALK - [CO_3^{2-}]/0.6$ (Yu et al., 2016). We assume that $[CO_3^{2-}]$
196 primarily responds to changing ΣCO_2 but also discuss the moderating influence that alkalinity
197 may play on millennial and longer timescales. To create a representative time series for the
198 Brazil Margin sites for comparison to other paleoclimate proxies, we combined the $[CO_3^{2-}]$
199 results from each core into a single time series and then plotted the results using a simple 3-point
200 running mean.
201
202 Table 1. Parameters for estimating modern Brazil Margin $[CO_3^{2-}]$

Core	Water depth (m)	Potential Temp (°C)	S	PO_4^{3-} (μmol/kg)	SiO_3^{2-} (μmol/kg)	ALK (μmol/kg)	Avg. ΣCO_2 (μmol/kg)	$[CO_3^{2-}]$ (μmol/kg)
78GGC	1820	3.81	34.90	1.7	30	2310 ± 5	2185 ± 7	94 ± 7
33GGC	2082	3.50	34.95	1.5	25	2312 ± 9	2171 ± 2	102 ± 7

203
204
205

206 **3. Results**

207

208 **3.1. $[CO_3^{2-}]$ Data**

209 Benthic foraminiferal $[CO_3^{2-}]$ time series for the Brazil Margin show similar overall
210 patterns on glacial-interglacial timescales (Figure 2). At 1800 m and 2100 m, $[CO_3^{2-}]$ is highest
211 during the late LGM (19-21 kyr BP), with values of 122±2 and 108±1 μmol/kg, respectively.
212 (Unless otherwise noted, the uncertainties stated here are standard errors.) Higher implied
213 $[CO_3^{2-}]$ values at 1800 m during the LGM are consistent with the presence of well ventilated
214 Glacial North Atlantic Intermediate Water above ~2 km water depth (Curry and Oppo, 2005; Yu
215 et al., 2008; Hoffman and Lund, 2012). At 18 kyr BP, $[CO_3^{2-}]$ began to decrease at both sites,
216 reaching a minimum of ~85 μmol/kg by 12 kyr BP, and then rebounding at ~10 kyr BP. At 2100
217 m water depth, the increase is abrupt and then levels off by 8 kyr BP whereas at 1800 m, $[CO_3^{2-}]$
218 continues to increase gradually throughout the Holocene. Given the more variable $[CO_3^{2-}]$ results
219 at 2100 m after 10 kyr BP, additional data points are necessary to better constrain the time series
220 during this interval. Nonetheless, the results from both cores converge to a similar $[CO_3^{2-}]$ value
221 (~100 μmol/kg) in the late Holocene. The core top results are similar to modern Brazil Margin
222 $[CO_3^{2-}]$ values at 1800 m and 2100 m (Figure 2b, d), even though the ALK and ΣCO_2 station data
223 used to calculate modern $[CO_3^{2-}]$ are well offshore of the Brazil Margin core sites, and the late
224 Holocene data are relatively sparse in each core.

225

226 Millennial scale changes in $[CO_3^{2-}]$ are apparent throughout the deglaciation. The largest
227 changes occurred during the LGM to HS1 transition, where $[CO_3^{2-}]$ decreased 22±2 μmol/kg at
228 1800 m and 21±5 μmol/kg at 2100 m (Figures 2 and 3). If we remove the low $[CO_3^{2-}]$ value in

229 the 2100 m record at ~15.5 kyr BP, the decrease in $[CO_3^{2-}]$ is 17±4 μmol/kg, within error of the
230 original estimate. During the HS1 to B-A transition, $[CO_3^{2-}]$ at 1800 m and 2100 m increased by
231 ~15 μmol/kg and then decreased by a similar amount at the beginning of Younger Dryas (YD:
232 11.5-12.9 kyr BP). The average $[CO_3^{2-}]$ record ($[CO_3^{2-}]_{AVG}$) shows a pattern similar to
233 individual time series (Figure 3). The main exception is the early Holocene, where deepening of
234 NCW apparently caused the individual records to diverge (see section 4.7).
235
236 **3.2. $[CO_3^{2-}]$ vs. $\%CaCO_3$**
237 Calcium carbonate results from 78GGC and 33GGC provide additional perspective on
238 changes in bottom water carbonate chemistry during the deglaciation (Figure 4). $\%CaCO_3$ values
239 ranged from 10-15% in the 20 to 16 kyr BP interval, followed by an increase to 40% by 10 kyr
240 BP, and then a slight decrease during the Holocene (Figure 4a, c). Thus, the long-term trend in
241 $\%CaCO_3$ is generally opposite that for $[CO_3^{2-}]$ in each core. The difference is due to dilution of
242 $CaCO_3$ by non-carbonate sedimentary components. $\%CaCO_3$ is suppressed during the LGM and
243 early deglaciation due to input of hemipelagic clays that yield sedimentation rates an order of
244 magnitude higher than during the Holocene (Tessin & Lund, 2013). During the early
245 deglaciation, however, sedimentation rates in 78GGC and 33GGC are nearly constant. The 1-
246 3% decrease in $\%CaCO_3$ during HS1 may therefore reflect calcium carbonate dissolution (Figure
247 4b, d). The synchronous decrease in $\%CaCO_3$ and $[CO_3^{2-}]$ during HS1 suggests that higher
248 ΣCO_2 at 1800-2100 m water depth resulted in modest calcite dissolution, which would tend to
249 increase alkalinity locally.
250
251

4. Discussion

Our primary aim in reconstructing the carbonate ion history at the Brazil Margin is to elucidate changes in South Atlantic carbon cycling. In particular, our goal is to determine whether the mid-depth Atlantic acted as a temporary reservoir of carbon during millennial-scale stadial events of the last deglaciation, as predicted by modeling results (Schmittner and Lund, 2015). The records presented here have high temporal resolution from the LGM through Younger Dryas (78GGC ~ 210 yr; 33GGC ~ 320 yr), allowing us to infer changes in carbon storage on millennial timescales. Below we discuss changes in mid-depth South Atlantic [CO_3^{2-}] during HS1, the B-A, and YD, as well as broader, glacial-interglacial trends, with the purpose of highlighting variability across a range of timescales. We also discuss the most likely mechanisms behind the observed changes in [CO_3^{2-}], use mass balance constraints to assess the remineralized vs. preformed components of the HS1 $\delta^{13}C$ signal, and make an initial estimate of carbon sequestration in the mid-depth Atlantic during HS1.

4.1. Millennial-scale signal driven by variable carbon storage

Both Brazil Margin time series suggest [CO_3^{2-}] decreased by ~20 μmol/kg during HS1 (Figure 2). Given that [CO_3^{2-}] is a function of both alkalinity and total dissolved inorganic carbon, it is possible the [CO_3^{2-}] signal reflects decreasing ALK. We believe this is unlikely, however, given that average oceanic alkalinity would have a lagged response to any deglacial changes in carbonate preservation, particularly if they were related to sea level rise, the bulk of which occurred after HS1 (Clark et al., 2009). Additionally, %$CaCO_3$ at the Brazil Margin decreased slightly at 1800 m and 2100 m water depth during HS1 (Figure 4), which would

275 increase alkalinity locally, opposite the effect required to account for the [CO_3^{2-}] signal. Finally,
276 modeling results indicate that weakening of the AMOC increases alkalinity at mid-depths
277 (Figure 5). The continued export of $CaCO_3$ from the surface ocean and its dissolution in the deep
278 ocean, combined with a more sluggish circulation, increases [Ca^{2+}] and therefore alkalinity. The
279 modeled ALK increase at the Brazil Margin is approximately 20 μM, which yields an equivalent
280 increase in [CO_3^{2-}]. Thus, the reconstructed [CO_3^{2-}] decline during HS1 likely underestimates
281 the ΣCO_2 signal.
282
283 The mid-depth $\delta^{13}C$ anomalies at the Brazil Margin were most likely driven by
284 weakening of the AMOC (Lund et al., 2015; Oppo et al., 2015; Schmittner and Lund, 2015).
285 Therefore, the simplest explanation of the [CO_3^{2-}] signal also involves the AMOC, either through
286 higher preformed DIC values in the source region or accumulation of respired carbon due to
287 increased residence time of mid-depth waters. While the first option appears to be plausible, in
288 part because the decrease in Brazil Margin [CO_3^{2-}] and the initial increase in atmospheric CO_2
289 both occurred during HS1, closer examination of the records reveals that the [CO_3^{2-}] signal leads
290 atmospheric CO_2 by ~ 1 kyr (Figure 3). If air-sea gas exchange was responsible for increased
291 ΣCO_2 in the mid-depth Atlantic, then [CO_3^{2-}] at the Brazil Margin would lag or be
292 contemporaneous with atmospheric CO_2. The age error for the ice core CO_2 record at ~17 kyr
293 BP is ±80 years (1σ) (Sigl et al., 2016). The age error for the Brazil Margin data at 18 kyr BP is
294 ±250 years (1σ) (Tessin and Lund, 2013), which is primarily due to an assumed ± 200 year
295 uncertainty in surface water reservoir age. Reconciling the Brazil Margin and atmospheric CO_2
296 time series would require a 1000-year increase in reservoir age, an unrealistically large change
297 given the subtropical gyre location of the Brazil Margin sites (modern $\Delta R = 7 \pm 59$ years (1σ))

298 (Angulo et al., 2005). Furthermore, the increase in [CO_3^{2-}] at the end of HS1 is not matched by a
299 decrease in atmospheric CO_2 (Figure 3), suggesting that preformed DIC levels were not a
300 primary driver of millennial-scale [CO_3^{2-}] variability at the Brazil Margin.
301
302 **4.2. Temporary carbon storage driven by AMOC variability**
303 If AMOC weakening and accumulation of respired carbon drove the [CO_3^{2-}] signal, the
304 B/Ca records should display variability similar to proxies of the AMOC. The $^{231}Pa/^{230}Th$ record
305 of McManus et al. (2004) is commonly used as reference time series for AMOC variability.
306 Given the caveats associated with Pa/Th as a circulation proxy (e.g Gherardi et al., 2009; Hayes
307 et al., 2015), here we use it to assess the approximate timing of changes in the AMOC rather than
308 a quantitative measure of AMOC strength. Given that the overall pattern in Pa/Th is consistent
309 with other circulation proxies from the Atlantic (Chen et al., 2015; Tessin and Lund, 2013; Oppo
310 et al., 2015), we believe such an approach is reasonable. At the beginning of HS1, [CO_3^{2-}] at the
311 Brazil Margin decreased concomitantly with the rise in Pa/Th, suggesting that a weaker AMOC
312 not only reduced export of Pa from the North Atlantic but it also led to increased carbon storage
313 and lower [CO_3^{2-}] at the Brazil Margin (Figure 3). While Pa/Th remained relatively stable from
314 17 to 15 kyr BP, [CO_3^{2-}] in both Brazil Margin cores continued to decrease after 16 kyr BP,
315 which may reflect continued accumulation of respired carbon in a weakened AMOC state or a
316 delayed response to rising atmospheric CO_2. Results from the North Atlantic also show a
317 decrease in [CO_3^{2-}] at the onset of HS1 but the record lacks the necessary resolution to determine
318 whether [CO_3^{2-}] continued to decline from 17 to 15 kyr BP (Yu et al., 2010).
319
320 At the beginning of the B/A, when the AMOC was apparently reinvigorated, [CO_3^{2-}]

increased by 15 μmol/kg, implying that ΣCO_2 declined by ~25 μmol/kg (Figure 3). Vertical $\Delta^{14}C$ gradients in the tropical Atlantic also disappear at the onset of the B/A, consistent with a resumption of the AMOC and enhanced southward advection of ^{14}C enriched NCW (Chen et al., 2015). Later in the deglaciation, apparent weakening of the AMOC during the YD coincides with a decrease in $[CO_3^{2-}]$ of 10-15 μmol/kg (Figure 3). At the end of the YD, both Pa/Th and coral $\Delta^{14}C$ records imply the AMOC became reinvigorated once again (McManus et al., 2004; Chen et al., 2015), which should liberate respired carbon from the mid-depth Atlantic. While there was a modest increase in $[CO_3^{2-}]$ at the end of the YD, the signal appears to be muted by the overall glacial-interglacial shift in $[CO_3^{2-}]$, which is likely due to progressively higher preformed DIC values. Lower sedimentation rates and sampling resolution during the YD and early Holocene section of the Brazil Margin cores may also preclude detection of subtle millennial-scale signals during this time interval.

4.3. Spatial gradients in $[CO_3^{2-}]$ and $\delta^{13}C$ anomalies during HS1

Model results suggest that weakening of the AMOC should create a north-south gradient in $[CO_3^{2-}]$ anomalies during HS1, similar to that observed in $\delta^{13}C$ (Schmittner and Lund, 2015). Comparison of the Brazil Margin results with $[CO_3^{2-}]$ data from the tropical North Atlantic indicates there was a meridional gradient in carbonate ion anomalies during HS1, with larger anomalies in the North Atlantic (Figure 6). Although the $[CO_3^{2-}]$ signal in core VM28-122 was originally interpreted as CO_2 released from the deep sea (Yu et al., 2010), we instead suggest that it reflects a weaker AMOC and greater accumulation of respired carbon at mid-depth, as implied by model results (Figure 7).

While the timing and spatial pattern in [CO_3^{2-}] anomalies are broadly consistent with the expected response to AMOC weakening, inconsistencies between the model results and benthic foraminiferal records do exist. The modeled [CO_3^{2-}] decrease of 20-30 μmol/kg (Figure 7) agrees well with the Brazil Margin results but the model overestimates the observed [CO_3^{2-}] decrease in the tropical North Atlantic by a factor of two. The simulated $\delta^{13}C$ response in the North Atlantic is also larger than implied by observations (Schmittner and Lund, 2015). Either the AMOC didn't collapse entirely during HS1 or the use of preindustrial initial conditions amplifies the simulated [CO_3^{2-}] signal at the depth of VM28-122 (~1800 m). In the model simulations, VM28-122 sits in the core of NADW (Figure 7), whereas during the LGM, NCW was shallower in the water column (Curry and Oppo, 2005). As a result, the modeled change in [CO_3^{2-}] during an AMOC shutdown is likely too large for this location. The discrepancy in [CO_3^{2-}] signals may also be due to the lack of interactive carbonate sediment dissolution in the model. Dissolution of $CaCO_3$ under elevated levels of total DIC would increase alkalinity and therefore moderate the [CO_3^{2-}] response. Despite these factors, the observed north-south gradient in $\delta^{13}C$ and [CO_3^{2-}] anomalies is consistent with the accumulation of isotopically light carbon in the mid-depth Atlantic.

4.4. Preformed vs. remineralized $\delta^{13}C$ signal

The modeling results of Schmittner and Lund (2015) suggest that approximately 65% of the Brazil Margin $\delta^{13}C$ signal can be attributed to remineralized $\delta^{13}C$ ($\delta^{13}C_{Rem}$) and 35% to preformed $\delta^{13}C$ ($\delta^{13}C_{Pre}$) (Figure 8). A somewhat higher proportion of the negative $\delta^{13}C$ shift in the tropical North Atlantic is due to changes in $\delta^{13}C_{Rem}$ (~80%) (Figure 8). Assuming the [CO_3^{2-}] signal between the LGM (19-21 kyr BP) and early HS1 (16-17 kyr BP) was primarily the

result of remineralization, we can estimate the influence on $\delta^{13}C$ using the following mass balance equations:

$$(\delta^{13}C_{Final})(\Sigma CO_{2\ Final}) = (\delta^{13}C_{Added})(\Sigma CO_{2\ Added}) + (\delta^{13}C_{LGM})(\Sigma CO_{2\ LGM}) \quad \text{(eqn.1)}$$

$$\Sigma CO_{2\ Final} = \Sigma CO_{2\ Added} + \Sigma CO_{2\ LGM} \quad \text{(eqn. 2)}$$

where $\delta^{13}C_{Final}$ represents the $\delta^{13}C$ value after input of respired carbon, $\delta^{13}C_{LGM}$ is the mean $\delta^{13}C$ for the LGM time interval, and $\Sigma CO_{2\ Added}$ is the estimated ΣCO_2 change between the LGM and early HS1 based on the $[CO_3^{2-}]$ results (Table 2). We assume that $\delta^{13}C_{Added}$ is equal to the mean value for $\delta^{13}C$ for marine organic carbon for samples from 40°S to 80°N (-21±2‰) (2σ) (Goericke and Fry, 1994). Although we have no proxy estimate for $\Sigma CO_{2\ LGM}$, the mean ΣCO_2 for the modern global ocean below 1000 m water depth is 2270±50 μmol/kg (1σ) (Schmittner et al., 2013). We assume a similar value for the LGM but with a conservative ±100 μmol/kg uncertainty. Note that the exact choice for $\Sigma CO_{2\ LGM}$ has little influence on $\delta^{13}C_{Final}$ because of the modest relative error of ~5%.

Table 2. Mass balance parameters and results

	KNR159-5-78GGC[1]	KNR159-5-33GGC[1]	VM28-122[2]
Mean LGM $\delta^{13}C$ (‰)	1.03±0.01	0.77±0.02	1.1±0.04
$\Sigma CO_{2\ Added}$ (μmol/kg)	37±4	23±6	48±7
$\delta^{13}C_{Final}$ (‰)	0.68±0.10	0.55±0.16	0.64±0.12
Mean HS1 $\delta^{13}C$ (‰)	0.55±0.02	0.42±0.02	0.5±0.1

[1] $\delta^{13}C$ from Tessin and Lund (2013); [2] $\delta^{13}C$ from Oppo & Fairbanks (1987), Yu et al., 2010

The mass balance results imply that the most of the Brazil Margin $\delta^{13}C$ signal was due to

385 changes in $\delta^{13}C_{Rem.}$ For example, $\delta^{13}C_{Final}$ for 78GGC is 0.68‰, which means that ~75% of the
386 change between the LGM ($\delta^{13}C$=1.03‰) and early HS1 ($\delta^{13}C$=0.55‰) can be attributed to
387 remineralization. Taking into account the errors listed in Table 1, the proportion due to
388 remineralization ranges from 50% to 100%. A somewhat lower fraction of the HS1 $\delta^{13}C$ signal
389 in core 33GGC can be explained by changes in $\delta^{13}C_{Rem}$ (60%) but it is within error of the
390 78GGC results. In the North Atlantic, it appears that remineralization also caused ~75% of the
391 HS1 $\delta^{13}C$ signal, with the proportion ranging from 50% to 100%. Thus, the results from each
392 core show that remineralization played the primary role in setting the $\delta^{13}C$ tracer field at mid-
393 depths, consistent with our model results (Figure 8).
394
395 The remainder of the $\delta^{13}C$ signal at each site must be due to changes in $\delta^{13}C_{Pre.}$ We
396 estimate that the $\delta^{13}C_{Pre}$ signal was -0.13±0.11‰ for 78GGC, -0.13±0.16‰ for 33GGC, and
397 -0.14±0.16‰ for VM28-122. These values are similar to the modeled ~0.15‰ decrease in
398 $\delta^{13}C_{Pre}$ in the mid-depth Atlantic (Figure 8), which is driven by gas exchange with a ^{13}C-depleted
399 atmosphere and weakening of the biological pump triggered by shutdown of the AMOC, both of
400 which cause surface ocean $\delta^{13}C$ to decrease (Schmittner and Lund, 2015). The overall agreement
401 between the reconstructed and modeled values for $\delta^{13}C_{Rem}$ and $\delta^{13}C_{Pre}$ suggests: 1) weakening of
402 the AMOC drove changes in both remineralized and preformed $\delta^{13}C$ to yield the overall HS1
403 $\delta^{13}C$ anomalies, and 2) the majority of the $\delta^{13}C$ response was due to biological processes,
404 implying that $\delta^{13}C$ acted non-conservatively during HS1. Our results are consistent with previous
405 indications of non-conservative $\delta^{13}C$ behavior during the last deglaciation (e.g. Tessin and Lund,
406 2013; Oppo et al., 2015) and to our knowledge provide the first quantitative estimate of

407 preformed and remineralized $\delta^{13}C$ components using paired stable isotope and B/Ca results.

408

409 **4.5. Implications for atmospheric CO_2**

410 If a weakened AMOC resulted in greater carbon storage in the mid-depth Atlantic during
411 HS1 and YD, what is the fate of the sequestered carbon under a reinvigorated AMOC
412 circulation, and what are the implications for atmospheric CO_2? Two centennial scale ~10-15
413 ppm increases in atmospheric CO_2 occurred at ~14.8 and ~11.7 kyr BP (Marcott et al., 2014)
414 (Figure 3). Bauska et al. (2016) report minor shifts in the $\delta^{13}C$ of atmospheric-CO_2 associated
415 with the centennial-scale events. Given that the abrupt increases in CO_2 coincide with northern
416 hemisphere warming, SST may be the primary driver, with contributions from other secondary
417 inputs that moderate the $\delta^{13}C$ signal (Bauska et al., 2016). The relative timing of the centennial
418 scale events with abrupt reinvigoration of the AMOC implies there is tight coupling between the
419 overturning circulation and pCO_2 variability (Marcott et al., 2014). The resumption of the
420 AMOC may trigger abrupt liberation of CO_2 to the atmosphere as a result of changes in
421 terrestrial carbon storage (Kohler et al. 2005). Alternatively, Chen et al. (2015) hypothesized the
422 abrupt increases in CO_2 were due to flushing of remineralized carbon out of the mid-depth
423 Atlantic during intervals of reinvigorated overturning. Consistent with this idea, our data suggest
424 ΣCO_2 decreased at the end of HS1 (Figure 3). However, our data also show that carbon
425 accumulated at mid-depths during the course of HS1, which would tend to draw down
426 atmospheric CO_2. Thus, it is unlikely that the mid-depth Atlantic acted as a net source of carbon
427 to the atmosphere across the combined HS1 to B-A interval. Instead, we suggest that
428 sequestration in the mid-depth Atlantic muted the rate of atmospheric CO_2 rise during HS1.
429 Upon the resumption of overturning during the B-A, we speculate the accumulated carbon was

then released, rectifying the deficit in atmospheric CO_2 caused by the weakened AMOC state. A similar process may have occurred during the YD, where weakening of the AMOC resulted in carbon sequestration and lower [CO_3^{2-}] at mid-depths (Figure 3). Presumably, reinvigoration of the AMOC at the end of the YD caused the carbon to be released, which may contribute to the observed abrupt shift in atmospheric CO_2 at 11.7 kyr BP (Marcott et al., 2014; Chen et al., 2015).

Our results imply that other factors, such as weakening of the biological pump (Schmittner and Lund, 2015; Hertzberg et al., 2016) or release of CO_2 from the Southern Ocean (Anderson et al., 2009), must have caused the rise in atmospheric CO_2 during HS1 and the YD, overcoming the temporary carbon sink in the mid-depth Atlantic. The combined effects of a weakened biological pump and release of respired carbon may explain why atmospheric CO_2 increased in a stepwise pattern, instead of a steady monotonic fashion throughout the deglaciation. AMOC-related changes in the carbon cycle cannot explain the overall increase in pCO_2; additional processes must be involved in maintaining high CO_2 levels during the B-A and Holocene when the AMOC was robust and the global preformed nutrient budget would presumably favor carbon sequestration in the ocean interior (Galbraith and Jaccard, 2015).

4.6. Quantifying ΣCO_2 Storage

To assess whether the release of respired carbon could have contributed to the centennial-scale increase in atmospheric CO_2 at the end of HS1, we use the B/Ca records from the Brazil Margin and tropical North Atlantic to generate an initial quantitative estimate of ΣCO_2 storage. We assume that ALK remained constant from the LGM to HS1. As noted above, this will likely yield a minimum estimate for ΣCO_2 given that 1) carbonate dissolution would increase alkalinity

453 and minimize the [CO_3^{2-}] signal, and 2) enhanced residence time of mid-depth water during HS1
454 would lead to accumulation of alkalinity associated with the hard tissue pump (Figure 5). We
455 conservatively assume a depth range of 1750 ± 250 m and an area of 5.2±0.3 × 10^{13} m^2 (~60°N
456 to ~35°S), which is the approximate volume encompassed by negative $\delta^{13}C$ anomalies in a
457 simulated shutdown of the AMOC (Schmittner and Lund, 2015). Using a seawater density of
458 1026 kg/m^3, this volume is equivalent to a total mass of 9.3±1.4 × 10^{19} kg. Assuming an average
459 decrease in [CO_3^{2-}] from the LGM to HS1 of 30±10 μmol/kg, we estimate an average increase in
460 ΣCO_2 of 50±17 μmol/kg, or a total carbon storage of 56±21 Pg.
461
462 If 56 Pg of carbon were released directly to the atmosphere, it would be equivalent to a
463 pCO_2 change of ~26 ppm (1 ppm ~ 2.12 Gt C; Keeling & Whorf, 2005). A portion of this
464 carbon would be re-absorbed by the upper ocean, however, so the net influence on atmospheric
465 CO_2 would be substantially less. Over the past two centuries, 50% of the carbon released through
466 fossil fuel burning has been absorbed by the ocean (Sabine et al., 2004). To first order, we would
467 expect a similar proportion to be absorbed by the ocean during centennial-scale CO_2 events of
468 the last deglaciation. Determining the actual fate of the stored carbon will require detailed
469 modeling efforts to assess the proportions released to the atmosphere and redistributed to other
470 ocean basins. Additional remineralized organic carbon may have been stored in the deep Atlantic
471 (>2500 m) prior to HS1 (Hoogakker et al., 2015; Howe et al., 2016), which should also be
472 considered in assessing redistribution of carbon between various reservoirs. Given the
473 uncertainties in our estimate of ΣCO_2 storage, additional high-resolution B/Ca records from a
474 range of depths and locations will be necessary to refine estimates for the Atlantic. Nevertheless,
475 our initial estimate suggests that: 1) significant quantities of carbon were stored in the mid-depth

476 Atlantic during HS1 and the YD, and 2) the mid-depth reservoir should to be taken into account
477 when interpreting the atmospheric CO_2 signal during the last deglaciation.
478
479 **4.7. Glacial-Interglacial Changes in [CO_3^{2-}]**
480 The dominant long-term trend in the Brazil Margin records is a steady decrease in [CO_3^{2-}]
481 from the LGM to the early Holocene (Figure 2). The most likely explanation for the signal is
482 changing preformed ΣCO_2 due to air-sea exchange with an atmosphere with progressively higher
483 CO_2 levels. Although air-sea gas exchange is an unlikely driver for the millennial scale decreases
484 in [CO_3^{2-}] during HS1 and the YD, over the course of the deglaciation such a process could lead
485 to lower [CO_3^{2-}] at depths influenced by NCW. For example, after the rapid decline in [CO_3^{2-}]
486 during HS1, [CO_3^{2-}] rebounds during the B-A, but does not fully recover to LGM values (Figure
487 3). This suggests that preformed ΣCO_2 in the mid-depth Atlantic increased as a result of greater
488 CO_2 absorption from the atmosphere. Between the LGM and B-A, atmospheric CO_2 increased
489 by ~50 ppm. A decline in global ocean alkalinity may also contribute to the long-term [CO_3^{2-}]
490 trend at the Brazil Margin. Although there was little apparent change in carbonate weathering
491 (Foster and Vance, 2006) and deep-sea $CaCO_3$ burial (Catubig et al., 1998) on glacial-
492 interglacial timescales, flooding of continental shelves late in the deglaciation would facilitate
493 deposition in carbonate banks and coral reefs, removing ALK and DIC in a 2:1 ratio (Sigman
494 and Boyle, 2000). Thus, a portion of the deglacial [CO_3^{2-}] decline in the Brazil Margin records
495 may reflect ALK removal.
496
497 If the long-term [CO_3^{2-}] trend at the Brazil Margin responded primarily to atmospheric
498 CO_2 and global changes in alkalinity then we would expect little change in [CO_3^{2-}] once

499 atmospheric CO_2 and sea level stabilized in the early Holocene. While this is largely the case at
500 2100 m water depth, [CO_3^{2-}] at 1800 m steadily increased from 10 to 2 kyr BP (Figure 2). One
501 possible explanation of the depth-dependent signal is a shift in watermass geometry. During the
502 LGM, [CO_3^{2-}] was ~10 μmol/kg higher at 1800 m than at 2100 m (Figure 3), which is consistent
503 with Brazil Margin $\delta^{13}C$ profiles that show the core of NCW was located at 1600-1800 m water
504 depth (Lund et al., 2015). By the early Holocene, however, [CO_3^{2-}] was 10-15 μmol/kg *lower* at
505 1800 m than 2100 m and vertical $\delta^{13}C$ profiles suggest the core of NCW had migrated to 2000-
506 2500 m (Lund et al., 2015). Thus, the 1800 m core site would have been more heavily influenced
507 by high [CO_3^{2-}] NCW during the LGM than during the early Holocene, potentially accounting
508 for the different temporal trend at this water depth. Additional factors, such as enhanced
509 Labrador Sea Water formation (Hoogakker et al., 2011) and the appearance of Upper
510 Circumpolar Deep Water at the Brazil Margin during the mid-Holocene (Lund et al., 2015),
511 likely influence the long-term evolution of the mid-depth [CO_3^{2-}] signal. Detailed vertical
512 transects of B/Ca from the Brazil Margin and elsewhere are necessary to more fully assess the
513 roles of rising atmospheric CO_2, global alkalinity, and vertical migration of watermass
514 boundaries on the glacial-interglacial [CO_3^{2-}] signal.
515
516 **5. Conclusions**
517 Carbon isotope anomalies were a ubiquitous feature of the mid-depth Atlantic during
518 HS1 yet the driver of the anomalies has remained enigmatic. Recent modeling efforts suggest
519 the $\delta^{13}C$ signal is driven by weakening of the AMOC which increases the residence time of mid-
520 depth waters, allowing for the accumulation of isotopically light respired carbon. Here we
521 examined the ΣCO_2 history at ~2 km water depth in South Atlantic using two high resolution

B/Ca time series spanning the last ~25 kyr. Our records show that $[CO_3^{2-}]$ decreased by 20-25 μmol/kg during HS1, concomitant with apparent weakening of the AMOC. The records also show that $[CO_3^{2-}]$ increased ~15 μmol/kg during the B-A and decreased ~15 μmol/kg during the YD, suggesting a tight coupling between mid-depth $[CO_3^{2-}]$ and AMOC state. Given the inverse relationship between $[CO_3^{2-}]$ and ΣCO_2, we infer that ΣCO_2 increased during millennial-scale stadial events of the last deglaciation. We also present model results which indicate weakening of the AMOC increases alkalinity at mid-depths, implying the $[CO_3^{2-}]$ time series likely underestimate the ΣCO_2 signal.

Comparison of the $[CO_3^{2-}]$ results from the Brazil Margin and tropical North Atlantic indicates there was a meridional gradient in $[CO_3^{2-}]$ anomalies during HS1, similar to the pattern observed in $\delta^{13}C$ records. Our mass balance estimates suggest approximately ¾ of the $\delta^{13}C$ signal at 27°S and 12°N was due to remineralization, highlighting the non-conservative nature of $\delta^{13}C$ behavior during HS1. Given that simulated weakening of the AMOC produces analogous spatial patterns in $[CO_3^{2-}]$ and $\delta^{13}C$, we infer the dominant driving mechanism behind the observed signals is the accumulation of remineralized carbon.

Our results imply the mid-depth Atlantic sequestered carbon during HS1 and the YD, both times of rising atmospheric CO_2. Thus, alternative processes, such as weakening of the biological pump (Hertzberg et al., 2016) or outgassing from the Southern Ocean (Anderson et al., 2009) must account for the overall increase in atmospheric CO_2 during stadial events. Reinvigoration of the AMOC may release stored carbon from the mid-depth Atlantic and contribute to abrupt centennial-scale increases in CO_2 at the end of HS1 and the YD. The

545 decrease in ΣCO_2 at the Brazil Margin at the beginning of the B-A is consistent with this
546 scenario. We also present a preliminary estimate of carbon storage in the mid-depth Atlantic
547 comparable to the quantity required to account for the rise in atmospheric CO_2 at the end of HS1.
548 Determining the fate of the stored carbon will require detailed modeling efforts to assess
549 partitioning between atmospheric and oceanic reservoirs.
550
551 **6. Acknowledgements**
552
553 We would like to thank Graham Nash at Australian National University for help with
554 sample processing and Jennifer Hertzberg for reviewing a pre-submission version of this
555 manuscript. Two anonymous reviewers also made substantive comments that greatly improved
556 the final version. We are grateful to the WHOI core lab for sample collection and archiving.
557 This work was supported by NSF grant OCE-1404915 to DL and by ARC Discovery Project
558 DP140101393 and Future Fellowship FT140100993 to JY. The data presented in this paper are
559 available at: https://www.ncdc.noaa.gov/paleo/study/22090.

References

Anderson, R. F., Ali, S., Bradtmiller, L. I., Nielsen, S. H., Fleisher, M. Q., Anderson, B. E., et al. (2009). Wind-Driven Upwelling in the Southern Ocean and the Deglacial Rise in Atmospheric CO_2. *Science, 323*(5920), 1443-1448.

Angulo, R. J., de Souza, M. C., Reimer, P. J., & Sasaoka, S. K. (2005). Reservoir Effect of the Southern and Southeastern Brazilian Coast. *Radiocarbon, 47*(1), 67-73.

Annan, J., & Hargreaves, J. (2013). A New Global Reconstruction of Temperature Changes at the Last Glacial Maximum. *Climate of the Past, 9*(1), 367-376.

Bauska, T. K., Baggenstos, D., Brook, E. J., Mix, A. C., Marcott, S. A., Petrenko, V. V., et al. (2016). Carbon Isotopes Characterize Rapid Changes in Atmospheric Carbon Dioxide During the Last Deglaciation. *Proceedings of the National Academy of Sciences of the United States of America, 113*(13), 3465-3470.

Broecker, W. S., & Maier-Reimer, E. (1992). The Influence of Air and Sea Exchange on the Carbon Isotope Distribution in the Sea. *Global Biogeochemical Cycles, 6*(3), 315-320.

Broecker, W. S., Peng, T., & Beng, Z. (1982). *Tracers in The Sea* Lamont-Doherty Geological Observatory, Columbia University.

Catubig, N. R., Archer, D. E., Francois, R., deMenocal, P., Howard, W., and Yu, E-F. (1998). Global deep-sea burial rate of calcium carbonate during the last glacial maximum. *Paleoceanography, 13*, 298-310.

Chen, T., Robinson, L. F., Burke, A., Southon, J., Spooner, P., Morris, P. J., et al. (2015). Synchronous Centennial Abrupt Events in the Ocean and Atmosphere During the Last Deglaciation. *Science, 349*(6255), 1537-1541.

Clark, P. U., Dyke, A. S., Shakun, J. D., Carlson, A. E., Clark, J., Wohlfarth, B., et al. (2009). The Last Glacial Maximum. *Science, 325*(5941), 710-714.

Curry, W. B., Duplessy, J., Labeyrie, L., & Shackleton, N. J. (1988). Changes in the Distribution of $\delta^{13}C$ of Deep Water ΣCO_2 Between the Last Glaciation and the Holocene. *Paleoceanography, 3*(3), 317-341.

Curry, W. B., & Oppo, D. W. (2005). Glacial Water Mass Geometry and the Distribution of $\delta^{13}C$ of ΣCO_2 in the Western Atlantic Ocean. *Paleoceanography, 20*(1).

Dokken, T. M., & Jansen, E. (1999). Rapid Changes in the Mechanism of Ocean Convection During the Last Glacial Period. *Nature, 401*(6752), 458-461.

Duplessy, J., Shackleton, N., Fairbanks, R., Labeyrie, L., Oppo, D., & Kallel, N. (1988). Deepwater Source Variations During the Last Climatic Cycle and Their Impact on the Global Deepwater Circulation. *Paleoceanography, 3*(3), 343-360.

Foster, G. L., and Vance, D. (2006) Negligible glacial-interglacial variation in continental chemical weathering rates. *Nature, 444*, 918-921.

Galbraith, E. D., & Jaccard, S. L. (2015). Deglacial Weakening of the Oceanic Soft Tissue Pump: Global Constraints from Sedimentary Nitrogen Isotopes and Oxygenation Proxies. *Quaternary Science Reviews, 109*, 38-48.

Gherardi, J., Labeyrie, L., Nave, S., Francois, R., McManus, J. F., & Cortijo, E. (2009). Glacial-Interglacial Circulation Changes Inferred from $^{231}Pa/^{230}Th$ Sedimentary Record in the North Atlantic Region. *Paleoceanography, 24*(2).

Goericke, R., & Fry, B. (1994) Variations of marine plankton $\delta^{13}C$ with latitude, temperature, and dissolved CO_2 in the world ocean. *Global Biogeochemical Cycles, 8*, 85-90.

Hayes, Christopher T., et al. (2015). ^{230}Th and ^{231}Pa on GEOTRACES GA03, the US GEOTRACES North Atlantic Transect, and Implications for Modern and Paleoceanographic Chemical Fluxes. *Deep Sea Research Part II: Topical Studies in Oceanography* 116, 29-41.

Hertzberg, J. E., Lund, D. C., Schmittner, A., and Srkrivanek, A. (2016) Evidence for a biological pump driver of atmospheric CO_2 rise during Heinrich Stadial 1. *Geophysical Research Letters*, doi:10.1002/2016GL070723.

Hodell, D. A., & Curtis, J. H. (2008). Oxygen and Carbon Isotopes of Detrital Carbonate in North Atlantic Heinrich Events. *Marine Geology, 256*(1), 30-35.

Hoffman, J., & Lund, D. (2012). Refining the Stable Isotope Budget for Antarctic Bottom Water: New Foraminiferal Data from the Abyssal Southwest Atlantic. *Paleoceanography, 27*(1).

Hoogakker, Babette AA, et al. (2011). "Dynamics of North Atlantic Deep Water Masses during the Holocene." *Paleoceanography* 26.4

Howe, Jacob NW, Piotrowski, A. M., Noble, T. L., Mulitza, S., Chiessi, C. M. & Bayon, G. (2016). North Atlantic Deep Water production during the Last Glacial Maximum. *Nature Communications*, doi:10.1038/ncomms11765.

Köhler, P., Joos, F., Gerber, S. & Knutti, R. (2005). Simulated changes in vegetation distribution, land carbon storage, and atmospheric CO_2 in response to a collapse of the North Atlantic thermohaline circulation. *Clim. Dyn*. 25, 689–708.

Kroopnick, P. (1985). The Distribution of $\delta^{13}C$ of ΣCO_2 in the World Oceans. *Deep Sea Research Part A. Oceanographic Research Papers, 32*(1), 57-84.

Lewis, E., Wallace, D., & Allison, L. J. (1998). *Program Developed for CO_2 System Calculations* Carbon Dioxide Information Analysis Center, Managed by Lockheed Martin Energy Research Corporation for the US Department of Energy Tennessee.

Lourantou, A. et al. (2010) Constraint on the CO_2 rise by new atmospheric carbon isotopic measurements during the last deglaciation, *Global Biogeochemical Cycles, 24*, GB2015, doi:10.1029/2009GB003545.

Lund, D., Tessin, A., Hoffman, J., & Schmittner, A. (2015). Southwest Atlantic Water Mass Evolution During the Last Deglaciation. *Paleoceanography, 30*(5), 477-494.

Lynch-Stieglitz, J., Stocker, T. F., Broecker, W. S., & Fairbanks, R. G. (1995). The Influence of Air-Sea Exchange on the Isotopic Composition of Oceanic Carbon: Observations and Modeling. *Global Biogeochemical Cycles, 9*(4), 653-665.

Marcott, S. A., Bauska, T. K., Buizert, C., Steig, E. J., Rosen, J. L., Cuffey, K. M., et al. (2014). Centennial-Scale Changes in the Global Carbon Cycle During the Last Deglaciation. *Nature, 514*(7524), 616-619.

McManus, J. F., Francois, R., Gherardi, J., Keigwin, L. D., & Brown-Leger, S. (2004). Collapse and Rapid Resumption of Atlantic Meridional Circulation Linked to Deglacial Climate Changes. *Nature, 428*(6985), 834-837.

McManus, J. F., Oppo, D. W., & Cullen, J. L. (1999). A 0.5-Million-Year Record of Millennial-Scale Climate Variability in the North Atlantic. *Science, 283*(5404), 971-975.

Oppo, D. W., Curry, W. B., & McManus, J. F. (2015). What do Benthic $\delta^{13}C$ and $\delta^{18}O$ Data Tell us About Atlantic Circulation During Heinrich Stadial 1? *Paleoceanography, 30*(4), 353-368.

Rickaby, R., & Elderfield, H. (2005). Evidence from the High-Latitude North Atlantic for Variations in Antarctic Intermediate Water Flow During the Last Deglaciation. *Geochemistry, Geophysics, Geosystems, 6*(5).

Sabine, C. L. et al. (2004) The oceanic sink for anthropogenic CO_2. *Science, 305*, 367-371.

Schmitt, J., Schneider, R., Elsig, J., Leuenberger, D., Lourantou, A., Chappellaz, J., et al. (2012). Carbon Isotope Constraints on the Deglacial CO_2 Rise from Ice Cores. *Science 336*(6082), 711-714.

Schmittner, A., Gruber, N., Mix, A., Key, R., Tagliabue, A., & Westberry, T. (2013). Biology and Air–Sea Gas Exchange Controls on the Distribution of Carbon Isotope Ratios ($\delta^{13}C$) in the Ocean. *Biogeosciences, 10*(9), 5793-5816.

Schmittner, A., & Lund, D. (2015). Early Deglacial Atlantic Overturning Decline and its Role in Atmospheric CO_2 Rise Inferred from Carbon Isotopes ($\delta^{13}C$). *Climate of the Past, 11*(2),

135-152.

Schneider, B., Leduc, G., & Park, W. (2010). Disentangling Seasonal Signals in Holocene Climate Trends by Satellite-Model-Proxy Integration. *Paleoceanography, 25*(4).

Schneider, R., Dahmke, A., Kölling, A., Müller, P., Schulz, H., & Wefer, G. (1992). Strong Deglacial Minimum in the $\delta^{13}C$ Record from Planktonic Foraminifera in the Benguela Upwelling Region: Palaeoceanographic Signal or Early Diagenetic Imprint? *Geological Society, London, Special Publications, 64*(1), 285-297.

Shakun, J. D., Clark, P. U., He, F., Marcott, S. A., Mix, A. C., Liu, Z., et al. (2012). Global Warming Preceded by Increasing Carbon Dioxide Concentrations During the Last Deglaciation. *Nature, 484*(7392), 49-54.

Sigl, M., Cole-Dai, J. , Ferris, D., Fudge, T.J., McConnell, J.R., Welten, K., Winstrup, M., Woodruff, T.E., Brook, E.J., Buizert, C., Dunbar, N., Iverson, N., Koffman, B., Maselli, O.J., McGwire, K., Muscheler, R., Pasteris, D.R., Sowers, Sowers, T.A. and Taylor, K. C. (2016). The WAIS-Divide deep ice core WD2014 chronology - Part 1: Annual layer counting (31-0 ka BP). *Climate of the Past Discussions, 12*, 769-786.

Sigman, D. M., & Boyle, E. A. (2000). Glacial/Interglacial Variations in Atmospheric Carbon Dioxide. *Nature, 407*(6806), 859-869.

Tessin, A., & Lund, D. (2013). Isotopically Depleted Carbon in the Mid-Depth South Atlantic During the Last Deglaciation. *Paleoceanography, 28*(2), 296-306.

Thornalley, D. J., Elderfield, H., & McCave, I. N. (2010). Intermediate and Deep Water Paleoceanography of the Northern North Atlantic Over the Past 21,000 Years. *Paleoceanography, 25*(1).

Waelbroeck, C., Skinner, L., Labeyrie, L., Duplessy, J., Michel, E., Vazquez Riveiros, N., et al. (2011). The Timing of Deglacial Circulation Changes in the Atlantic. *Paleoceanography, 26*(3)

Weaver, A. J., Eby, M., Fanning, A. F., & Wiebe, E. C. (1998). Simulated Influence of Carbon Dioxide, Orbital Forcing and Ice Sheets on the Climate of the Last Glacial Maximum. *Nature, 394*(6696), 847-853.

Yu, J., & Elderfield, H. (2005). B/Ca in Foraminiferal Calcium Carbonate and its Potential as a Paleo-pH Proxy. Paper Presented at the *AGU Fall Meeting Abstracts.*

Yu, J., & Elderfield, H. (2007). Benthic Foraminiferal B/Ca Ratios Reflect Deep Water Carbonate Saturation State. *Earth and Planetary Science Letters, 258*(1), 73-86.

Yu, J., Broecker, W. S., Elderfield, H., Jin, Z., McManus, J., & Zhang, F. (2010). Loss of Carbon from the Deep Sea Since the Last Glacial Maximum. *Science, 330*(6007), 1084-1087.

741
742 Yu, J., et al. (2016). Sequestration of Carbon in the Deep Atlantic during the Last Deglaciation.
743 *Nature Geoscience*, doi:10.1038/NGEO2657.
744
745 Zahn, R., Schönfeld, J., Kudrass, H., Park, M., Erlenkeuser, H., & Grootes, P. (1997).
746 Thermohaline Instability in the North Atlantic During Meltwater Events: Stable Isotope
747 and Ice-Rafted Detritus Records from Core SO75-26KL, Portuguese Margin.
748 *Paleoceanography, 12*(5), 696-710.
749
750 Zahn, R., & Stüber, A. (2002). Suborbital Intermediate Water Variability Inferred from Paired
751 Benthic Foraminiferal Cd/Ca and $\delta^{13}C$ in the Tropical West Atlantic and Linking with
752 North Atlantic Climates. *Earth and Planetary Science Letters, 200*(1), 191-205.
753
754 Zeebe, R. E., & Wolf-Gladrow, D. A. (2001). *CO_2 in Seawater: Equilibrium, Kinetics, Isotopes*
755 Gulf Professional Publishing.

Figure captions

Figure 1. Locations of cores used in this study (white circles) overlain on a cross-section of carbonate ion concentration (in μmol/kg) from World Ocean Circulation Experiment (WOCE) A17 (Schlitzer 2015). Contour intervals are 10 μmol/kg. The sites are influenced primarily by high [CO_3^{2-}] North Atlantic Deep Water (NADW) and to lesser extent low [CO_3^{2-}] Upper Circumpolar Deep Water (UCDW). The inset map shows the location of the A17 section relative to the core sites (white circles). Note that hydrographic data closer to the core sites was used to estimate the modern carbonate ion values depicted in Figure 2 (see Methods).

Figure 2. Brazil Margin $\delta^{13}C$ and B/Ca records spanning the LGM through late Holocene. **A)** *C. wuellerstorfi* $\delta^{13}C$ data for KNR159-5-78GGC, including the average value at each stratigraphic level (thin blue line), a 3000-year running mean from 2 to 16 kyr BP, and a 1000-year running mean from 16 to 25 kyr BP (thick black lines). A wider averaging window was necessary from 2 to 16 kyr BP due to the lower sedimentation rates in the late deglaciation and Holocene. Stable isotope and radiocarbon data are from Tessin and Lund (2013) with calibrated dates as in Lund et al. (2015). **B)** Benthic B/Ca data for KNR159-5-78GGC (right y-axis), including the average value at each stratigraphic level (thin blue line), running mean values as in panel A, and ± 1 SE uncertainties (shaded area). Carbonate ion concentrations (left y-axis) were estimated using a core top calibration of 1.14 μmol/mol B/Ca per μmol/kg [CO_3^{2-}], with a calibration uncertainty of 5 μmol/kg = 1σ (Yu et al. 2016), shown as a the blue-grey error bar. Note that data points in core 78GGC at 73 & 77 cm (red circles) come from a bioturbated section of the core (see text for details). **C and D)** Benthic $\delta^{13}C$ and B/Ca data for KNR159-5-33GGC.

779 The averaging window in C is a 4000-year running mean from 2 to 16 kyr BP and a 2000-year
780 running mean from 16 to 25 kyr BP. Red squares in panels B and D are estimates of modern
781 [CO_3^{2-}] for the Brazil Margin sites. Vertical red bars are ± 1σ uncertainties. The vertical grey
782 bars in each panel mark the HS1 (14.5-17.5 kyr BP) and YD (12.9-11.6 kyr BP) intervals.
783
784 **Figure 3**. Atmospheric CO_2, deep North Atlantic $^{231}Pa/^{230}Th$ and Brazil Margin carbonate ion
785 results. **A)** Atmospheric CO_2 record (Marcott et al., 2014) with updated WD2014 age scale (Sigl
786 et al., 2016). Note y-axis is reversed. **B)** Brazil Margin [CO_3^{2-}] records for cores 78GGC (blue
787 circles) and 33GGC (red circles) and a 3-point running mean of the combined 78GGC and
788 33GGC records (black line). **C)** Sedimentary $^{231}Pa/^{230}Th$ data for OCE326-GGC5 (33°N, 4.5
789 km) including ^{238}U based values (purple circles) and ^{232}Th based values (green circles). The solid
790 green bar and blue bar delineate the HS1 (14.5-17.5 kyr BP) and YD intervals (11.5-12.9 kyr
791 BP), respectively. The Pa/Th and [CO_3^{2-}] results are consistent with a weakened AMOC during
792 HS1, strengthening during the B-A, and then weakening during the YD.
793
794 **Figure 4**. Brazil Margin [CO_3^{2-}] (blue lines) and %$CaCO_3$ records (orange lines). [CO_3^{2-}] is
795 plotted as in Figure 2 and %$CaCO_3$ is plotted as a three-point running mean. **A)** [CO_3^{2-}] and
796 %$CaCO_3$ records for KNR159-5-78GGC spanning 2 to 25 kyr BP. **B)** Zoomed in view of
797 panel A spanning 15 to 20 kyr BP. **C) and D)** same as panels A and B but for KNR159-5-
798 33GGC. The long-term trends in %$CaCO_3$ reflect variable sedimentation rate at the Brazil
799 Margin due to input of hemipelagic clay (Tessin and Lund, 2013) while the narrower
800 windows highlight short-term changes that are more likely dependent on ΣCO_2.
801

802 **Figure 5.** Simulated Atlantic Ocean alkalinity response due to a freshwater forcing induced
803 AMOC shutdown (Schmittner and Lund, 2015). **A)** Alkalinity for the preindustrial control run.
804 **B)** Alkalinity 2500 years after AMOC shutdown. **C)** The difference between the preindustrial
805 control and the shutdown state.
806
807 **Figure 6**. Brazil Margin and tropical North Atlantic B/Ca records spanning the LGM to late
808 Holocene. **A)** Benthic B/Ca data for KNR159-5-78GGC (blue circles). **B)** Benthic B/Ca data for
809 VM28-122 (red circles). [CO_3^{2-}] decreased ~20 μmol/kg at 27°S compared to ~30 μmol/kg at
810 12°N. The lower sedimentation rate for VM28-122 (7 cm/kyr during the deglaciation compared
811 to 35 cm/kyr for 78GGC) likely yields a relatively muted B/Ca signal in the North Atlantic.
812
813 **Figure** 7. Simulated response of $\delta^{13}C$ (left-hand column) and [CO_3^{2-}] (right-hand column) in the
814 Atlantic due to a freshwater forcing induced AMOC shutdown (Schmittner and Lund, 2015). **A**
815 **and B)** $\delta^{13}C$ and [CO_3^{2-}] for the Atlantic based on preindustrial initial conditions. Note that
816 NADW sits deeper in the water column than would be expected for the LGM given the boundary
817 conditions. **C and D)** $\delta^{13}C$ and [CO_3^{2-}] 2500 years after AMOC shutdown. **E and F)** The $\delta^{13}C$
818 and [CO_3^{2-}] anomalies (difference between post-AMOC shutdown and preindustrial values).
819 Both $\delta^{13}C$ and [CO_3^{2-}] show largest decreases in the North Atlantic, with progressively smaller
820 anomalies moving southward. The black circles mark the location of Brazil Margin cores,
821 including the mid-depth sites in white, while the red circle marks the sill depth and latitude
822 associated with V28-122 (Yu et al., 2010).
823

Figure 8. Simulated changes in $\Delta\delta^{13}C_{pre}$ and $\Delta\delta^{13}C_{rem}$ due to a freshwater forcing induced shutdown of the AMOC (Schmittner and Lund, 2015). A) Zonally averaged $\Delta\delta^{13}C_{pre}$ for the Atlantic basin. The approximate location of the mid-depth Brazil Margin cores are noted with white circles. B) Zonally averaged $\Delta\delta^{13}C_{rem}$ for the Atlantic basin. C) Average $\Delta\delta^{13}C$ (black), $\Delta\delta^{13}C_{pre}$ (green), and $\Delta\delta^{13}C_{rem}$ (red) at 28°S, using vertical profiles from 30°W to 45°W. The remineralized signal is approximately double the preformed signal at the depth of the Brazil Margin cores. Note that the anomalies are calculated 1000 years after the AMOC collapse to facilitate comparison to the HS1 $\delta^{13}C$ anomalies, which were determined using the 16-17 kyr BP time window.

Figure 1.

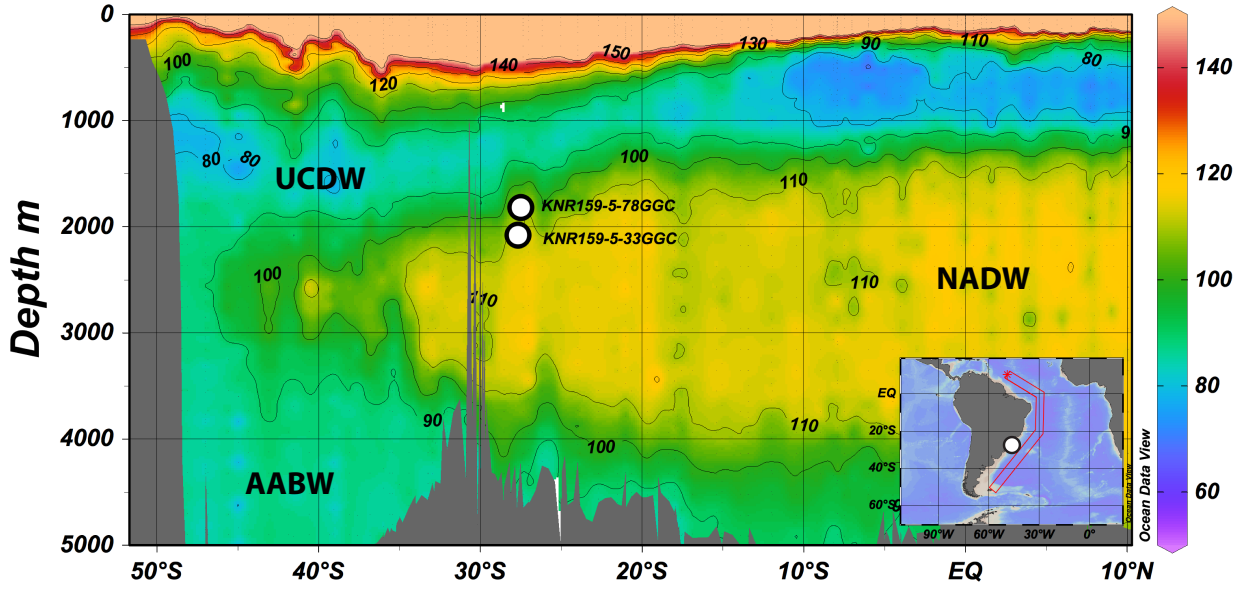
Depth m
0
1000
2000
3000
4000
5000
50°S
40°S
30°S
20°S
10°S
EQ
10°N
UCDW
NADW
AABW
KNR159-5-78GGC
KNR159-5-33GGC
100
120
140
150
130
90
110
80
60
EQ
20°S
40°S
60°S
90°W
60°W
30°W
0°
Ocean Data View

Figure 2.

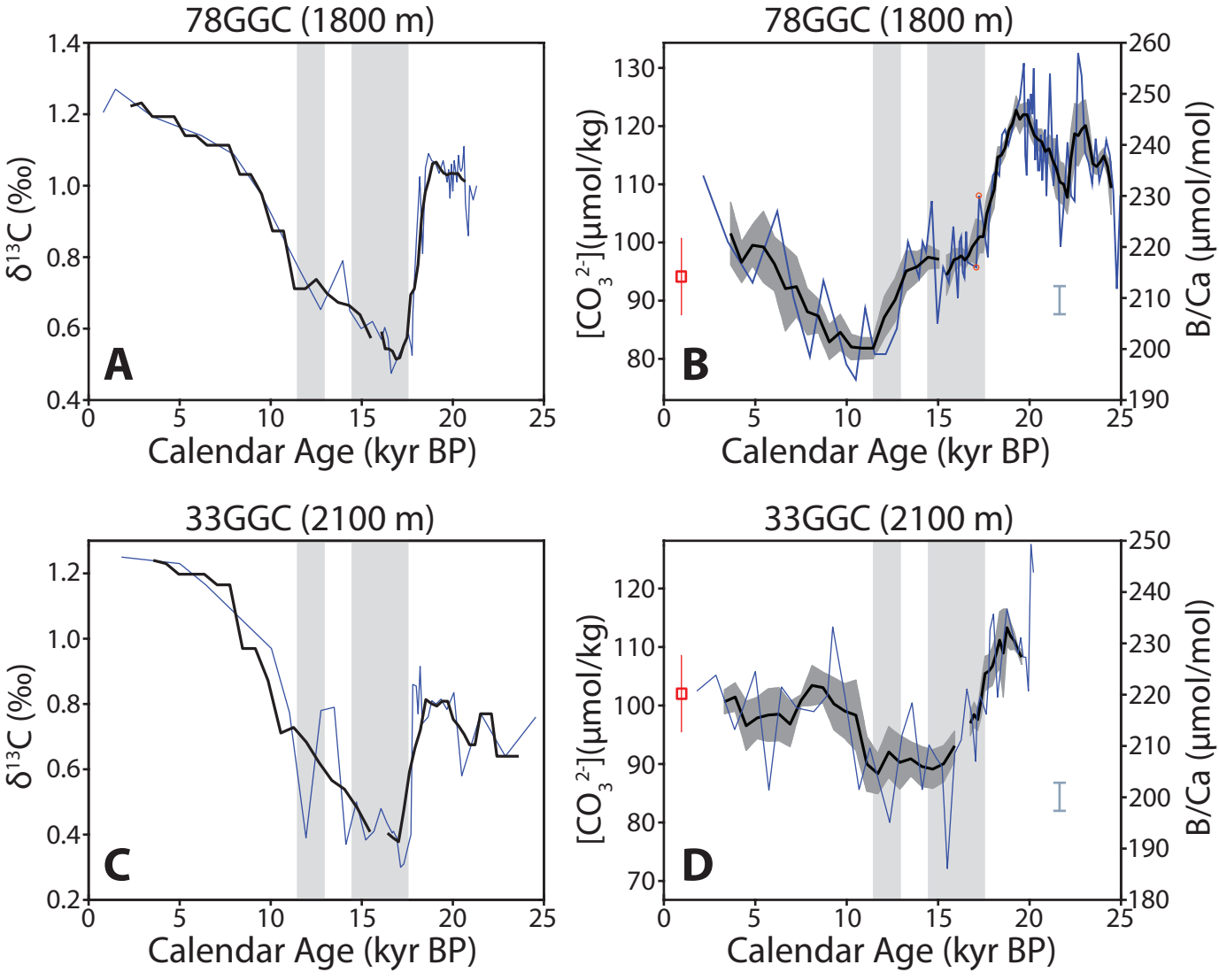
78GGC (1800 m)
δ13C (‰)
Calendar Age (kyr BP)
A
78GGC (1800 m)
[CO3 2-](µmol/kg)
B/Ca (µmol/mol)
Calendar Age (kyr BP)
B
33GGC (2100 m)
δ13C (‰)
Calendar Age (kyr BP)
C
33GGC (2100 m)
[CO3 2-](µmol/kg)
B/Ca (µmol/mol)
Calendar Age (kyr BP)
D

Figure 3.

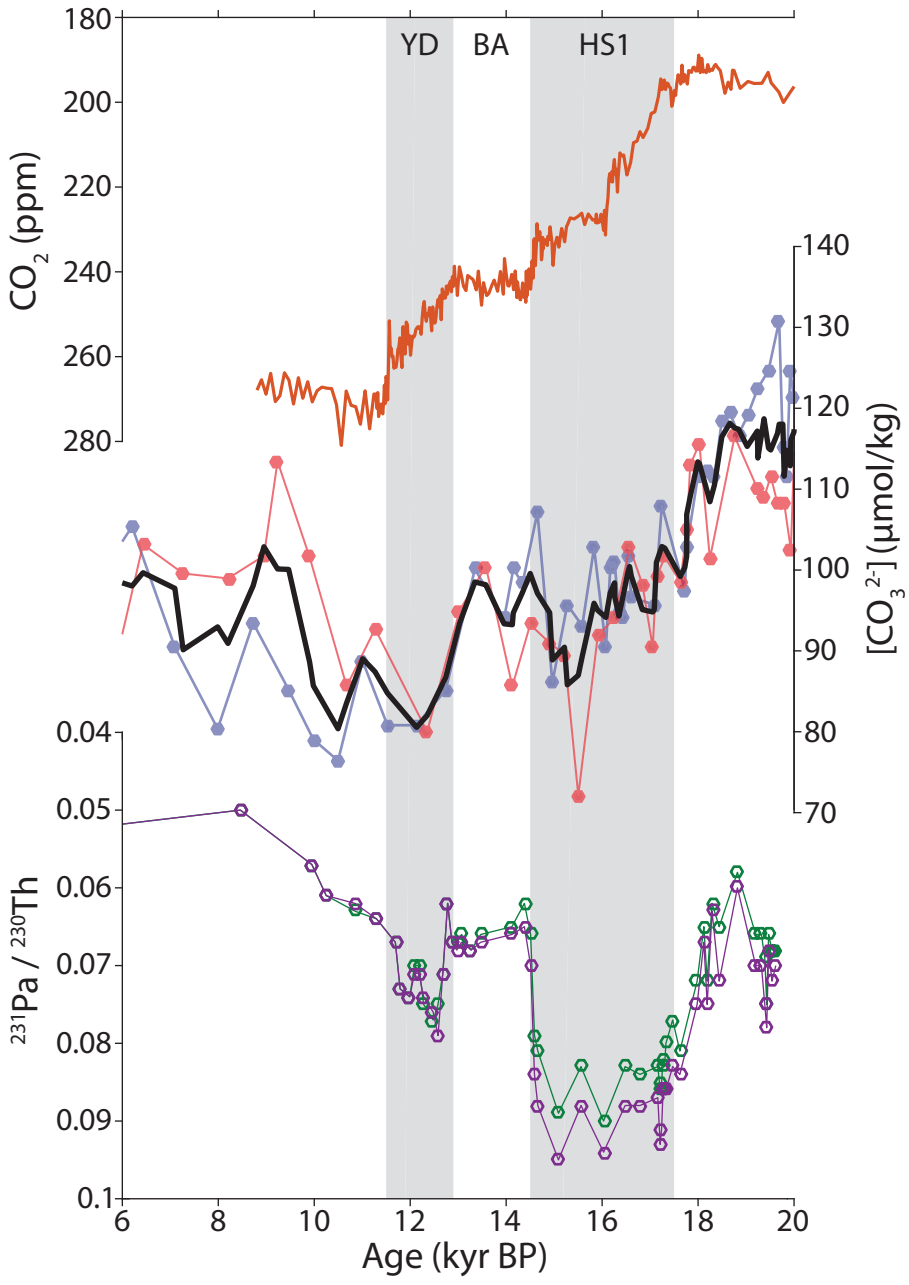
YD
BA
HS1
180
200
220
240
260
280
CO2 (ppm)
140
130
120
110
100
90
80
70
[CO3 2-] (µmol/kg)
0.04
0.05
0.06
0.07
0.08
0.09
0.1
231Pa / 230Th
6
8
10
12
14
16
18
20
Age (kyr BP)

Figure 4.

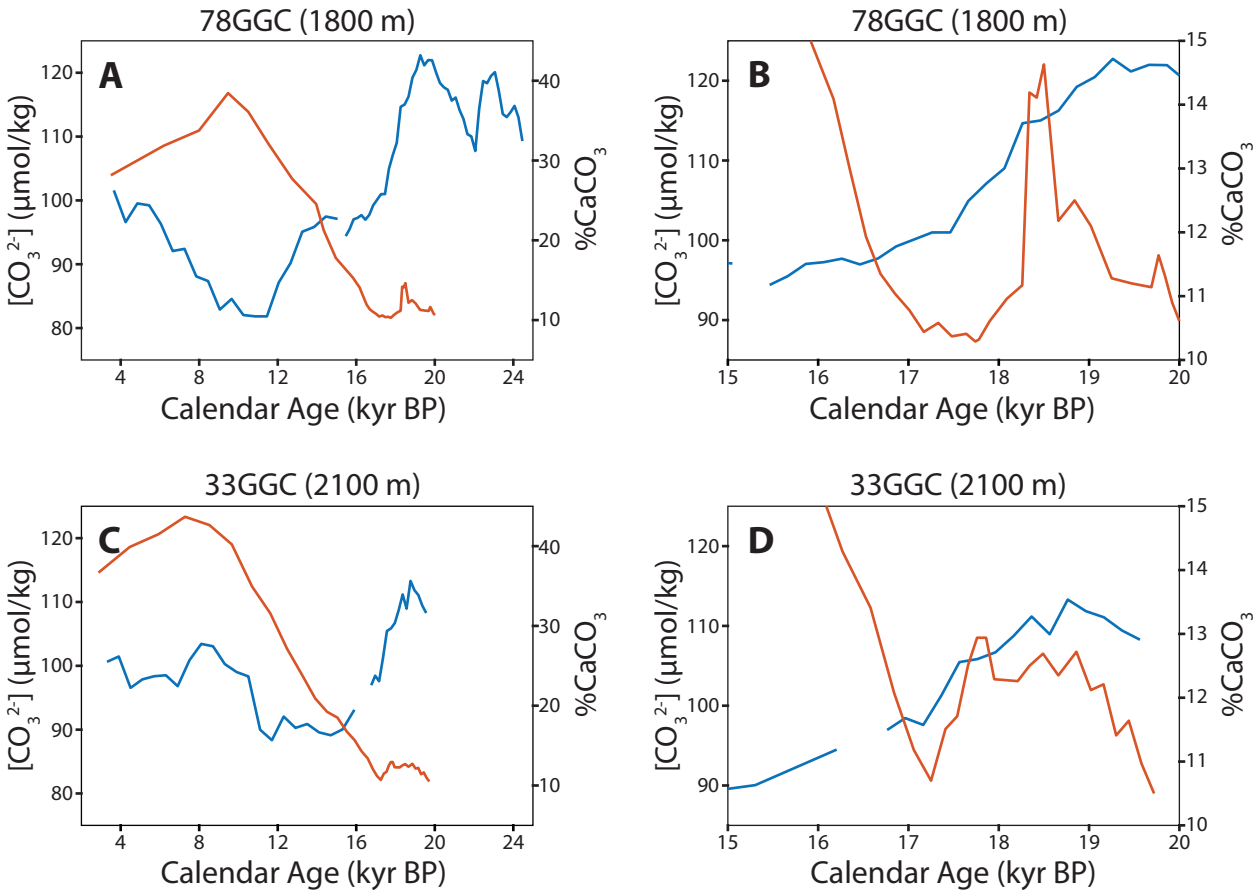
78GGC (1800 m)
A
[CO3 2-] (µmol/kg)
%CaCO3
Calendar Age (kyr BP)
78GGC (1800 m)
B
[CO3 2-] (µmol/kg)
%CaCO3
Calendar Age (kyr BP)
33GGC (2100 m)
C
[CO3 2-] (µmol/kg)
%CaCO3
Calendar Age (kyr BP)
33GGC (2100 m)
D
[CO3 2-] (µmol/kg)
%CaCO3
Calendar Age (kyr BP)

Figure 5.

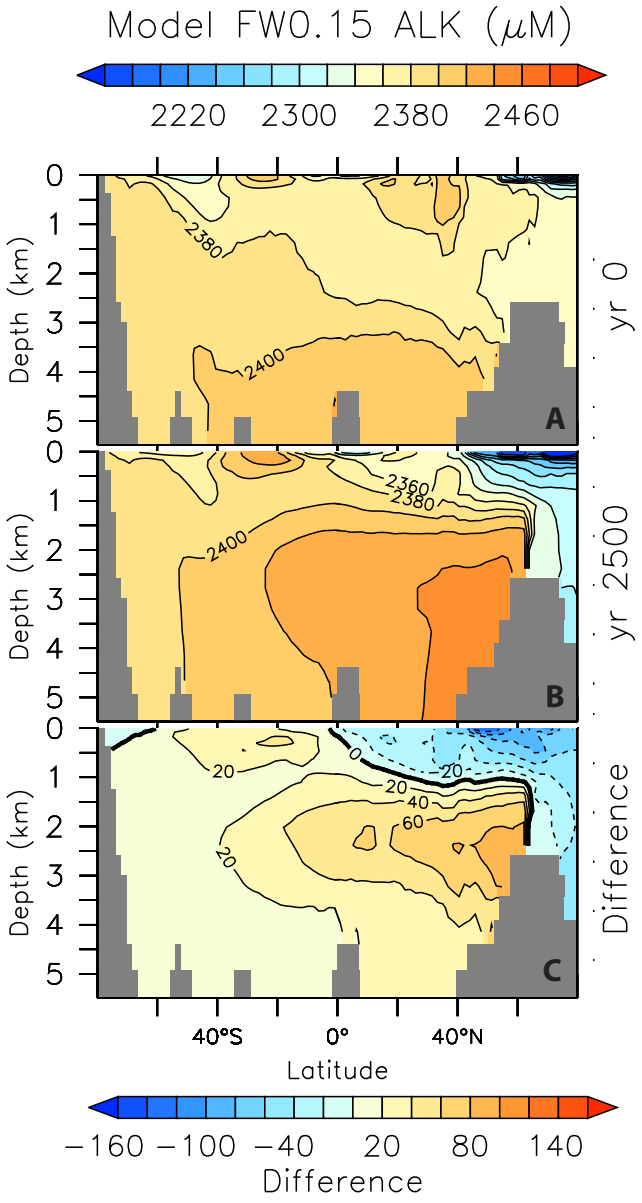
Model FW0.15 ALK (μM)
2220
2300
2380
2460
Depth (km)
0
1
2
3
4
5
2380
2400
A
yr 0
2360
2380
2400
B
yr 2500
20
0
20
20
40
60
20
C
Difference
40°S
0°
40°N
Latitude
−160
−100
−40
20
80
140
Difference

Figure 6.

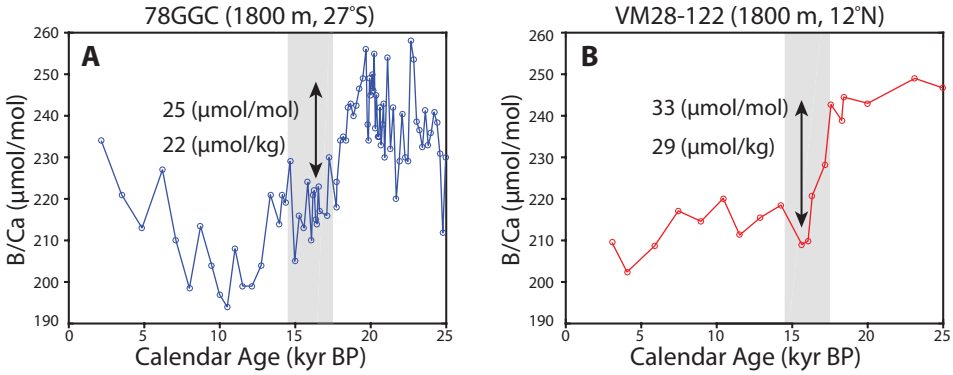
78GGC (1800 m, 27°S)
A
25 (µmol/mol)
22 (µmol/kg)
B/Ca (µmol/mol)
Calendar Age (kyr BP)
VM28-122 (1800 m, 12°N)
B
33 (µmol/mol)
29 (µmol/kg)
B/Ca (µmol/mol)
Calendar Age (kyr BP)

Figure 7.

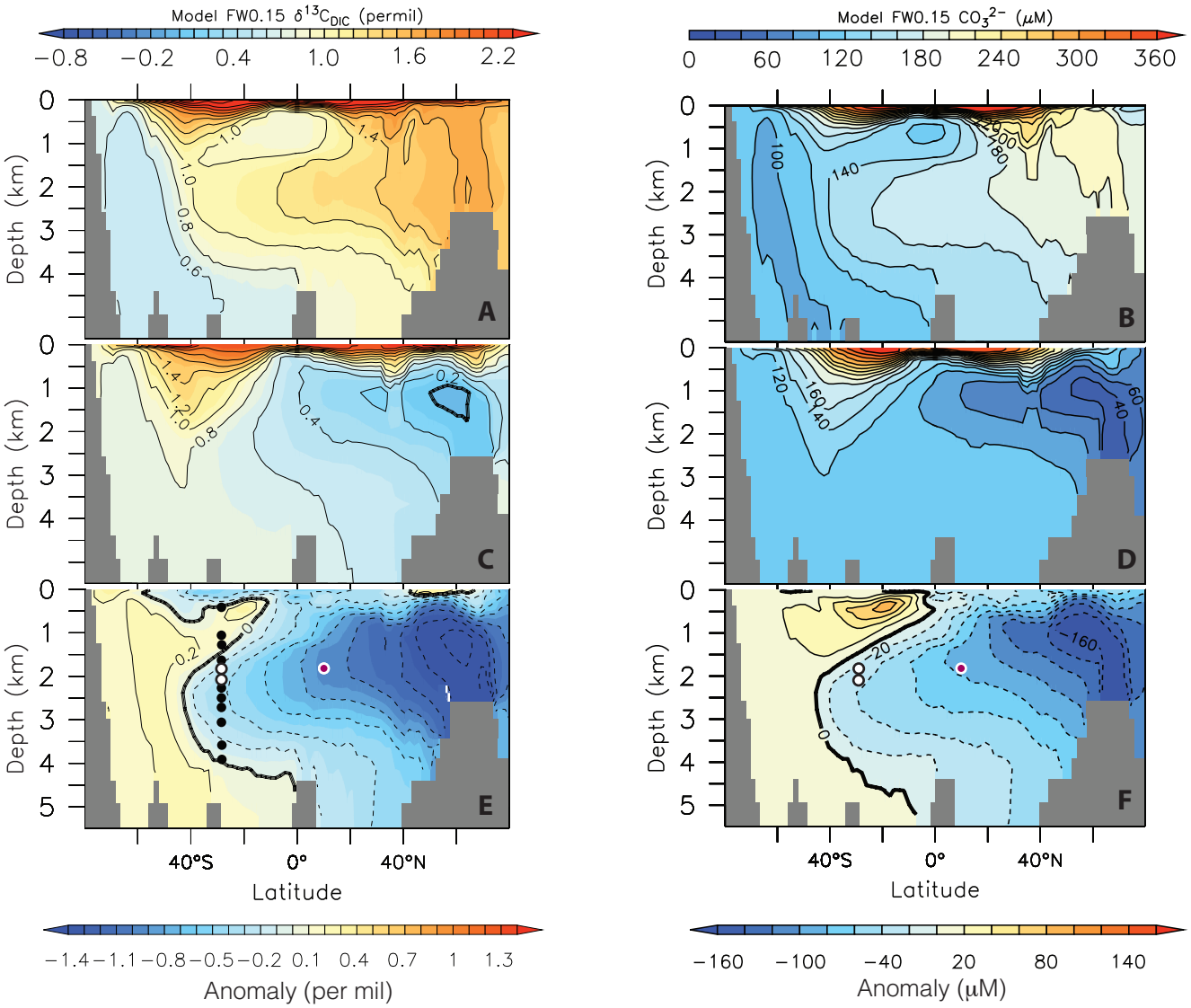
Model FW0.15 $\delta^{13}C_{DIC}$ (permil)
−0.8 −0.2 0.4 1.0 1.6 2.2
Model FW0.15 CO_3^{2-} (μM)
0 60 120 180 240 300 360
Depth (km)
A
B
C
D
E
F
40°S 0° 40°N
Latitude
−1.4 −1.1 −0.8 −0.5 −0.2 0.1 0.4 0.7 1 1.3
Anomaly (per mil)
−160 −100 −40 20 80 140
Anomaly (μM)

Figure 8.

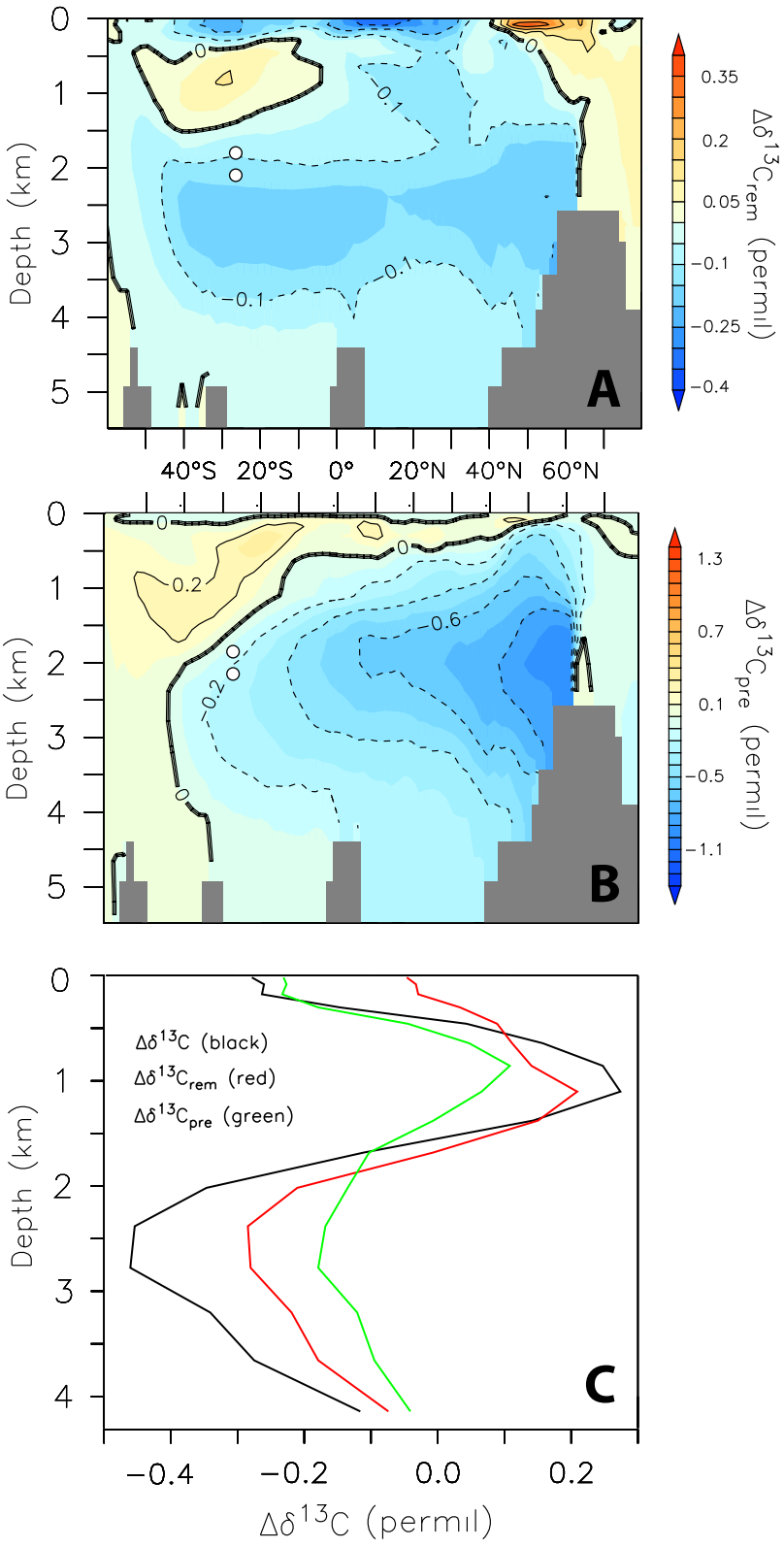
A
B
C
Depth (km)
40°S 20°S 0° 20°N 40°N 60°N
0.35
0.2
0.05
−0.1
−0.25
−0.4
Δδ13Crem (permil)
1.3
0.7
0.1
−0.5
−1.1
Δδ13Cpre (permil)
Δδ13C (black)
Δδ13Crem (red)
Δδ13Cpre (green)
−0.4 −0.2 0.0 0.2
Δδ13C (permil)